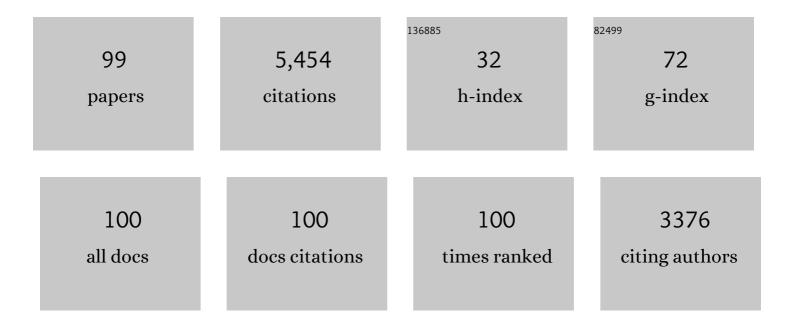
## Klaus Irmscher

List of Publications by Year in descending order

Source: https://exaly.com/author-pdf/2327079/publications.pdf Version: 2024-02-01



#	Article	IF	CITATIONS
1	On the bulk β-Ga2O3 single crystals grown by the Czochralski method. Journal of Crystal Growth, 2014, 404, 184-191.	0.7	556
2	3.8-MV/cm Breakdown Strength of MOVPE-Grown Sn-Doped <inline-formula> <tex-math notation="LaTeX"&gt;\$eta \$  &lt;/inline-formula&gt;-Ga<sub>2</sub>O<sub>3</sub>MOSFETs. IEEE Electron Device Letters, 2016, 37, 902-905.</tex-math </inline-formula>	2.2	468
3	Electrical properties of <i><math>\hat{l}^2</math></i> -Ga2O3 single crystals grown by the Czochralski method. Journal of Applied Physics, 2011, 110, .	1.1	442
4	Czochralski growth and characterization of βâ€Ga <sub>2</sub> O <sub>3</sub> single crystals. Crystal Research and Technology, 2010, 45, 1229-1236.	0.6	378
5	Schottky barrier height of Au on the transparent semiconducting oxide <i>β</i> -Ga2O3. Applied Physics Letters, 2012, 101, .	1.5	293
6	Scaling-Up of Bulk β-Ga <sub>2</sub> O <sub>3</sub> Single Crystals by the Czochralski Method. ECS Journal of Solid State Science and Technology, 2017, 6, Q3007-Q3011.	0.9	280
7	Experimental electronic structure of In <sub>2</sub> O <sub>3</sub> and Ga <sub>2</sub> O <sub>3</sub> . New Journal of Physics, 2011, 13, 085014.	1.2	273
8	Editors' Choice—Si- and Sn-Doped Homoepitaxial β-Ga <sub>2</sub> O <sub>3</sub> Layers Grown by MOVPE on (010)-Oriented Substrates. ECS Journal of Solid State Science and Technology, 2017, 6, Q3040-Q3044.	0.9	219
9	Structural properties of Si-doped β-Ga2O3 layers grown by MOVPE. Journal of Crystal Growth, 2014, 401, 665-669.	0.7	133
10	Hydrogen-related deep levels in proton-bombarded silicon. Journal of Physics C: Solid State Physics, 1984, 17, 6317-6329.	1.5	128
11	Semiconducting Sn-doped β-Ga2O3 homoepitaxial layers grown by metal organic vapour-phase epitaxy. Journal of Materials Science, 2016, 51, 3650-3656.	1.7	116
12	On the nature and temperature dependence of the fundamental band gap of In <sub>2</sub> O <sub>3</sub> . Physica Status Solidi (A) Applications and Materials Science, 2014, 211, 54-58.	0.8	96
13	Doping of Czochralski-grown bulk β-Ga2O3 single crystals with Cr, Ce and Al. Journal of Crystal Growth, 2018, 486, 82-90.	0.7	83
14	Czochralski-grown bulk β-Ga2O3 single crystals doped with mono-, di-, tri-, and tetravalent ions. Journal of Crystal Growth, 2020, 529, 125297.	0.7	78
15	Formation of the Z1,2 deep-level defects in 4H-SiC epitaxial layers: Evidence for nitrogen participation. Applied Physics Letters, 2002, 81, 4841-4843.	1.5	76
16	Evolution of planar defects during homoepitaxial growth of <i>β</i> -Ga2O3 layers on (100) substrates—A quantitative model. Journal of Applied Physics, 2016, 120, .	1.1	75
17	Ultra-wide bandgap, conductive, high mobility, and high quality melt-grown bulk ZnGa2O4 single crystals. APL Materials, 2019, 7, .	2.2	74
18	Step-flow growth in homoepitaxy of <b>β</b> -Ga2O3 (100)—The influence of the miscut direction and faceting. APL Materials, 2019, 7, .	2.2	73

#	Article	IF	CITATIONS
19	Influence of incoherent twin boundaries on the electrical properties of β-Ga2O3 layers homoepitaxially grown by metal-organic vapor phase epitaxy. Journal of Applied Physics, 2017, 122, .	1.1	69
20	Melt growth, characterization and properties of bulk In2O3 single crystals. Journal of Crystal Growth, 2013, 362, 349-352.	0.7	62
21	Preparation of deep UV transparent AlN substrates with high structural perfection for optoelectronic devices. CrystEngComm, 2016, 18, 3488-3497.	1.3	62
22	Step flow growth of <i>β</i> -Ga2O3 thin films on vicinal (100) <i>β</i> -Ga2O3 substrates grown by MOVPE. Applied Physics Letters, 2020, 116, .	1.5	59
23	Static Dielectric Constant of <i>β</i> -Ga <sub>2</sub> O <sub>3</sub> Perpendicular to the Principal Planes (100), (010), and (001). ECS Journal of Solid State Science and Technology, 2019, 8, Q3083-Q3085.	0.9	58
24	MgGa <sub>2</sub> O <sub>4</sub> as a new wide bandgap transparent semiconducting oxide: growth and properties of bulk single crystals. Physica Status Solidi (A) Applications and Materials Science, 2015, 212, 1455-1460.	0.8	56
25	Ultraviolet luminescence in AlN. Physica Status Solidi (B): Basic Research, 2011, 248, 1513-1518.	0.7	49
26	Bulk single crystals of β-Ga2O3 and Ga-based spinels as ultra-wide bandgap transparent semiconducting oxides. Progress in Crystal Growth and Characterization of Materials, 2021, 67, 100511.	1.8	47
27	Influence of nitrogen doping on the properties of 4H–SiC single crystals grown by physical vapor transport. Journal of Crystal Growth, 2003, 257, 75-83.	0.7	45
28	Temperature-dependent optical absorption of SrTiO <sub>3</sub> . Physica Status Solidi (A) Applications and Materials Science, 2015, 212, 1880-1887.	0.8	41
29	Effect of heat treatment on properties of melt-grown bulk In <sub>2</sub> O <sub>3</sub> single crystals. CrystEngComm, 2013, 15, 2220-2226.	1.3	40
30	<inline-formula> <tex-math notation="LaTeX">\$eta\$</tex-math> &lt;/inline-formula&gt;-Ga<sub>2</sub>O<sub>3</sub>Solid-State Devices for Fast Neutron Detection. IEEE Transactions on Nuclear Science, 2017, 64, 1574-1579.</inline-formula>	1.2	40
31	Ti- and Fe-related charge transition levels in $\hat{l}^2 \hat{a}^2 Ga 2O3$ . Applied Physics Letters, 2020, 116, .	1.5	37
32	Identification of a tri-carbon defect and its relation to the ultraviolet absorption in aluminum nitride. Journal of Applied Physics, 2013, 114, .	1.1	35
33	Vanadium centers in ZnTe crystals. I. Optical properties. Physical Review B, 1996, 53, 1907-1916.	1.1	31
34	Two inch diameter, highly conducting bulk <b> <i>β</i> </b> -Ga2O3 single crystals grown by the Czochralski method. Applied Physics Letters, 2022, 120, .	1.5	31
35	Heteroepitaxy of Ga <sub>2(1â€'x)</sub> In <sub>2x</sub> O <sub>3</sub> layers by MOVPE with two different oxygen sources. Crystal Research and Technology, 2014, 49, 552-557.	0.6	30
36	Melt growth and properties of bulk BaSnO <sub>3</sub> single crystals. Journal of Physics Condensed Matter, 2017, 29, 075701.	0.7	28

#	Article	IF	CITATIONS
37	Bulk β-Ga2O3 single crystals doped with Ce, Ce+Si, Ce+Al, and Ce+Al+Si for detection of nuclear radiation. Journal of Alloys and Compounds, 2020, 818, 152842.	2.8	28
38	Spectroscopic evidence and control of compensating native defects in doped ZnSe. Materials Science and Engineering B: Solid-State Materials for Advanced Technology, 2001, 80, 168-172.	1.7	27
39	Coloration and oxygen vacancies in wide band gap oxide semiconductors: Absorption at metallic nanoparticles induced by vacancy clustering—A case study on indium oxide. Journal of Applied Physics, 2014, 115, 053504.	1.1	27
40	The anisotropic quasi-static permittivity of single-crystal <b> <i>l²</i> </b> -Ga2O3 measured by terahertz spectroscopy. Applied Physics Letters, 2020, 117, .	1.5	27
41	Iron group impurities in Î'-FeSi2sstudied by EPR. Physical Review B, 1997, 55, 4417-4425.	1.1	26
42	Favourable growth conditions for the preparation of bulk AlN single crystals by PVT. CrystEngComm, 2020, 22, 1762-1768.	1.3	26
43	Impact of chamber pressure and Si-doping on the surface morphology and electrical properties of homoepitaxial (100) β-Ga <sub>2</sub> O <sub>3</sub> thin films grown by MOVPE. Journal Physics D: Applied Physics, 2021, 54, 034003.	1.3	26
44	Growth and Properties of Intentionally Carbonâ€Đoped GaN Layers. Crystal Research and Technology, 2020, 55, 1900129.	0.6	25
45	Vanadium centers in ZnTe crystals. II. Electron paramagnetic resonance. Physical Review B, 1996, 53, 1917-1926.	1.1	24
46	β-Ga2O3:Ce as a fast scintillator: An unclear role of cerium. Radiation Measurements, 2019, 121, 49-53.	0.7	23
47	Semiconductor scintillator development: Pure and doped β-Ga2O3. Optical Materials, 2020, 105, 109856.	1.7	22
48	Fast homoepitaxial growth of (100) $\hat{l}^2$ -Ga2O3 thin films via MOVPE. AIP Advances, 2021, 11, .	0.6	22
49	Polytype stability in nitrogen-doped PVT—grown 2″—4H–SiC crystals. Journal of Crystal Growth, 2005, 275, e451-e454.	0.7	21
50	Pyramidal inversion domain boundaries revisited. Applied Physics Letters, 2011, 99, .	1.5	21
51	Current Status of Carbonâ€Related Defect Luminescence in GaN. Physica Status Solidi (A) Applications and Materials Science, 2021, 218, 2100235.	0.8	21
52	Crystal growth and detector performance of large size High-purity Ge crystals. Materials Science in Semiconductor Processing, 2015, 39, 54-60.	1.9	20
53	Technology development of high purity germanium crystals for radiation detectors. Journal of Crystal Growth, 2020, 532, 125396.	0.7	18
54	Electron paramagnetic resonance of iron- and aluminum-related defects in silicon. Physical Review B, 1994, 49, 7964-7973.	1.1	15

#	Article	IF	CITATIONS
55	Tri-carbon defects in carbon doped GaN. Applied Physics Letters, 2018, 113, .	1.5	15
56	Tailoring the scintillation properties of β-Ga <sub>2</sub> O <sub>3</sub> by doping with Ce and codoping with Si. Optical Materials Express, 2019, 9, 3738.	1.6	15
57	Indium incorporation in homoepitaxial β-Ga2O3 thin films grown by metal organic vapor phase epitaxy. Journal of Applied Physics, 2019, 125, .	1.1	14
58	Raman scattering in heavily donor doped <b> <i>β</i> </b> -Ga2O3. Applied Physics Letters, 2020, 117, .	1.5	14
59	Approaching the high intrinsic electrical resistivity of NbO2 in epitaxially grown films. Applied Physics Letters, 2020, 116, 182103.	1.5	14
60	On the Determination of Deep Level Concentration Profiles by DLTS Measurements. Physica Status Solidi A, 1985, 91, 667-675.	1.7	13
61	Evolution of impurity incorporation during ammonothermal growth of GaN. Journal of Crystal Growth, 2016, 456, 51-57.	0.7	13
62	Electrical properties of (11-22) Si:AlGaN layers at high Al contents grown by metal-organic vapor phase epitaxy. Applied Physics Letters, 2020, 117, .	1.5	13
63	Impact of epitaxial strain on the ferromagnetic transition temperature of SrRuO3 thin films. Thin Solid Films, 2011, 519, 6264-6268.	0.8	12
64	Effects of doping on the electronic properties of semiconducting iron disilicide. Materials Science and Engineering B: Solid-State Materials for Advanced Technology, 1996, 37, 215-218.	1.7	11
65	Optical phonon modes, static and high-frequency dielectric constants, and effective electron mass parameter in cubic In2O3. Journal of Applied Physics, 2021, 129, .	1.1	11
66	Carbon pair defects in aluminum nitride. Journal of Applied Physics, 2019, 126, 215102.	1.1	10
67	A consistent picture of excitations in cubic BaSnO3 revealed by combining theory and experiment. Communications Materials, 2022, 3, .	2.9	10
68	Defect distribution in boron-reduced GaAs crystals grown by vapour-pressure-controlled Czochralski technique. Journal of Crystal Growth, 2008, 310, 1418-1423.	0.7	9
69	Bulk photovoltaic effect in carbon-doped gallium nitride revealed by anomalous surface photovoltage spectroscopy. Physical Review B, 2020, 101, .	1.1	9
70	Thermal conductivity of bulk <mml:math xmlns:mml="http://www.w3.org/1998/Math/MathML"&gt; <mml:mrow> <mml:msub> <mml:mi>In </mml:mi> <mml:n mathvariant="normal"&gt;O  <mml:mn>3 </mml:mn> </mml:n </mml:msub> </mml:mrow>  single crystals. Physical Review Materials, 2021, 5, .</mml:math 	nn>2 <td>nl:mŋ&gt;</td>	nl:mŋ>
71	Zinc gallate spinel dielectric function, band-to-band transitions, and Γ-point effective mass parameters. Applied Physics Letters, 2021, 118, .	1.5	9
72	Melt Growth and Physical Properties of Bulk LaInO 3 Single Crystals. Physica Status Solidi (A) Applications and Materials Science, 2021, 218, 2100016.	0.8	9

#	Article	IF	CITATIONS
73	Experimental Hall electron mobility of bulk single crystals of transparent semiconducting oxides. Journal of Materials Research, 2021, 36, 4746-4755.	1.2	9
74	Carbon doping of GaN: Proof of the formation of electrically active tri-carbon defects. Journal of Applied Physics, 2020, 127, 205701.	1.1	9
75	Structural and electrical properties of unintentionally doped 4H-SiC epitaxial layers—Grown by hot-wall CVD. Journal of Electronic Materials, 2001, 30, 207-211.	1.0	8
76	Calibration of the photoluminescence technique for measuring concentrations of shallow dopants in Ge. Journal of Applied Physics, 2012, 112, .	1.1	8
77	Electromechanical losses in carbon- and oxygen-containing bulk AlN single crystals. Solid State lonics, 2019, 343, 115072.	1.3	8
78	Terahertz electron paramagnetic resonance generalized spectroscopic ellipsometry: The magnetic response of the nitrogen defect in 4H-SiC. Applied Physics Letters, 2022, 120, .	1.5	8
79	Electroluminescence of Cr3+ and pseudo-Stark effect in β-Ga2O3 Schottky barrier diodes. Journal of Applied Physics, 2019, 126, 213104.	1.1	7
80	Resonant electronic Raman scattering from lr4+ ions in <i><math>\hat{l}^2</math></i> -Ga2O3. Journal of Applied Physics, 2022, 131, .	1.1	7
81	Toward Precise n-Type Doping Control in MOVPE-Grown β-Ga2O3 Thin Films by Deep-Learning Approach. Crystals, 2022, 12, 8.	1.0	7
82	Utilization of optical and electrical peculiarities of partially compensated zinc selenide. Materials Science in Semiconductor Processing, 2001, 4, 601-605.	1.9	6
83	Fingerprints of optical absorption in the perovskite LaInO3 : Insight from many-body theory and experiment. Physical Review B, 2021, 103, .	1.1	6
84	Recent progress in the development of β-Ga <sub>2</sub> O <sub>3</sub> scintillator crystals grown by the Czochralski method. Optical Materials Express, 2021, 11, 2488.	1.6	6
85	A carbon-doping related luminescence band in GaN revealed by below bandgap excitation. Journal of Applied Physics, 2021, 130, 055703.	1.1	6
86	Electron-paramagnetic-resonance identification of the manganese-gallium pair in silicon. Physical Review B, 1991, 44, 3678-3684.	1.1	5
87	Net acceptor concentration in ZnSe:Sb grown from vapor phase. Journal of Crystal Growth, 2002, 242, 155-160.	0.7	5
88	Structural and transport properties of SrRuO3 thin films grown by MOCVD on (001) SrTiO3 substrates: The role of built-in strain and extra phases. Materials Science and Engineering B: Solid-State Materials for Advanced Technology, 2011, 176, 647-652.	1.7	5
89	Brillouin zone center phonon modes in ZnGa2O4. Applied Physics Letters, 2020, 117, .	1.5	5
90	Characterization of Silicon Crystals Grown from Melt in a Granulate Crucible. Journal of Electronic Materials, 2020, 49, 5120-5132.	1.0	5

#	Article	IF	CITATIONS
91	Electronic characterization of the manganese–boron pair in silicon. Physica Status Solidi A, 1989, 116, 755-767.	1.7	4
92	Origin of brown coloration in top-seeded solution grown SrTiO <sub>3</sub> crystals. CrystEngComm, 2016, 18, 4580-4586.	1.3	4
93	Evenâ€Parity Excited States in Infrared Emission, Absorption, and Raman Scattering Spectra of Shallow Donor Centers in Silicon. Physica Status Solidi (B): Basic Research, 2019, 256, 1800514.	0.7	4
94	Elevated temperature spectroscopic ellipsometry analysis of the dielectric function, exciton, band-to-band transition, and high-frequency dielectric constant properties for single-crystal ZnGa2O4. Applied Physics Letters, 2022, 120, .	1.5	4
95	Hydrogen-related deep levels in proton-bombarded silicon. Journal of Physics C: Solid State Physics, 1985, 18, 4591-4591.	1.5	1
96	Experimental and Theoretical Investigation of the Surface Electronic Structure of ZnGa 2 O 4 (100) Singleâ€Crystals. Physica Status Solidi (B): Basic Research, 0, , 2100452.	0.7	1
97	Comment on "Electron spin resonance studies in β-FeSi2 crystals―[J. Appl. Phys.80, 1678 (1996)]. Journal of Applied Physics, 1997, 81, 8121-8123.	1.1	0
98	Photoelectron spectra of Al dopants in 4H–SiC. Materials Science and Engineering B: Solid-State Materials for Advanced Technology, 2003, 102, 284-288.	1.7	0
99	In-situ TEM Observations of Resistance Switching in Strontium Titanate Devices. Microscopy and Microanalysis, 2021, 27, 69-70.	0.2	0